31st Annual International Conference of the IEEE EMBS
Minneapolis, Minnesota, USA, September 2-6, 2009

Quantitative comparison of high-resolution MRI and myelin-stained histology of the human cerebral cortex

Sergey Osechinskiy and Frithjof Kruggel

Abstract— **The architectonic analysis of the human cerebral cortex is presently based on the examination of stained tissue sections. Recent progress in high-resolution magnetic resonance imaging (MRI) promotes the feasibility of an *in vivo* architectonic analysis. Since the exact relationship between the laminar fine-structure of a cortical MRI signal and histological cyto- and myeloarchitectonic staining patterns is not known, a quantitative study comparing high-resolution MRI to histological ground truth images is necessary for validating a future MRI based architectonic analysis. This communication describes an ongoing study comparing *post mortem* MR images to a myelin-stained histology of the brain cortex. After establishing a close spatial correspondence between histological sections and MRI using a slice-to-volume nonrigid registration algorithm, transcortical intensity profiles, extracted from both imaging modalities along curved trajectories of a Laplacian vector field, are compared via a cross-correlational analysis.**

I. INTRODUCTION

Histological examination still remains the gold standard for a precise characterization of the anatomy and pathology of neural tissue. Particularly, the cyto- and myeloarchitectonic parcellation of the brain cortex has relied over more than 100 years on histological staining of *post mortem* brain samples. Anatomical magnetic resonance imaging (MRI) presents a viable alternative to histology in applications where *in vivo* and/or three-dimensional (3D) imaging is needed. While the scale of analysis in MRI, which typically has a millimeter-scale resolution, is still far from reaching the micro-scale attainable in histology, a sub-millimeter voxel MRI resolution becomes increasingly more feasible due to progress in high-field MRI and high-resolution imaging hardware and protocols. If the sub-millimeter meso-scale turns to be adequate for characterization and delineation of cortical structural areas, high-resolution MRI will open new frontiers for an *in vivo* architectonic analysis of the cortex. Apart from the resolution scale, the two modalities (MRI and histology) also considerably differ in their image contrast mechanism. MRI offers a wide range of signal weighting contrast techniques, similarly to a vast variety of staining modalities in histology. MR image contrast has a complex origin that makes exact relationships between MRI and histology unclear; correlates of MRI findings with histology have to be studied and validated. In light of this, a quantitative study comparing high-resolution MRI to histological ground truth images appears to be essential for the assessment of the feasibility of an MRI based architectonic analysis of the brain cortex.

S. Osechinskiy and F. Kruggel are with the Department of Biomedical Engineering, University of California, Irvine CA 92697, USA {sosechin,fkruggel}@uci.edu

Comparison of high-resolution MRI with cortical histology was studied by several research groups. Fatterpekar et al. [1] qualitatively compared high-field (9.4 T) MR microscopy images of excised formalin-fixed brain sections to corresponding Nissl and myelin stained images. Fine-detailed MR images of various types of the cortex are published alongside of histological images, and convincingly demonstrate a close visual correspondence of a laminar structure in both modalities. Augustinack et al. [2] compared high-field (7 T) MR images of the entorhinal cortex in three formalin-fixed brains to Nissl histological sections, and found a good visual match of some cytoarchitectonic features. In both studies, however, no quantitative evaluation was provided. Eickhoff et al. [3] conducted a quantitative across-modality comparison of transcortical intensity profiles. Striate and extrastriate cortices were analyzed in five imaging modalities: *in vivo* T1-weighted MRI, *post mortem* T2-weighted MRI, two different types of myelin staining, and Nissl-type silver stain for neuron cell bodies. For each modality, the intensity profiles were sampled along linear transcortical profiles regularly spaced along the cortical layer. Intensity profiles were resampled to a unit length (length-normalized), and normalized to a zero mean and unit variance of intensity (z-normalized). The normalized profiles were compared statistically using Euclidean distance between inter-modal pairs as a similarity measure. The study [3] confirmed two key findings: 1) there is a close correspondence between *in vivo* T1 and (inverted) *post mortem* T2 profiles; 2) *in vivo* T1 cortical signals are significantly closer to myeloarchitectonic than to cytoarchitectonic profiles, but are best fitted by a weighted sum of both. Some limitations of the study [3] can be pointed out as areas of interest for further research: 1) spatial correspondence between inter-modal image pairs was established manually without registration; 2) many images originated from different brain samples; 3) only one region of the brain (visual cortex) was studied; 4) linear transcortical profiles were used instead of curvilinear profiles (the latter are believed to better follow the laminar organization of the cortex).

Our project deals with the quantitative comparison of *post mortem* MR images to myelin-stained sections of the cortex. We consider as novel contributions of the work described here: 1) we use a nonlinear registration procedure for achieving a cross-modal spatial correspondence; 2) a new application is found for a cross-correlational technique that was introduced in astronomy; 3) a novel combination of several techniques is applied to cross-modality comparison of intensity profiles; 4) an empirical evaluation of techniques

978-1-4244-3296-7/09/$25.00 ©2009 IEEE

is conducted on samples from several distinct regions of the cortex. The methodology is briefly outlined in the rest of this paragraph, and is described in more detail in next section. 1) Both MRI and histology originate from the same brain sample. 2) A close spatial correspondence between histological sections and MRI is established using a slice-to-volume nonrigid registration algorithm. 3) On registered slices, several regions of interest (ROI) covering the cortical band are selected for profiling. Anatomical attribution of ROIs to main sulcal landmarks is traced by an expert neuroanatomist using the 3D MR image. 4) Within a ROI in both imaging modalities, transcortical intensity profiles are extracted along curved trajectories of a Laplacian vector field. 5) Profiles are pre-processed, length-normalized, and z-normalized. 6) Template profiles are constructed from blocks of sufficiently similar adjacent histological profiles. 7) Template profiles are compared to MRI profiles via a cross-correlational analysis.

II. MATERIALS AND METHODS

Brain preparation and imaging: An isolated left brain hemisphere obtained from a routine autopsy was fixated in 4% paraformaldehyde. High-resolution MR images were acquired on a Bruker 3T Medspec 100 system using a T_1-weighted 3D-MDEFT protocol (FOV $179.2 \times 89.6 \times 179.2\,mm$, matrix $512 \times 256 \times 256$, voxel size $0.35 \times 0.35 \times 0.7\,mm$, scanning time 12 h). The white-grey matter contrast of the MR images is inverted due to fixation in formalin, which makes it similar to the contrast in histological images. After MRI scanning, the brain sample was cut on a macrotome into ten coronal blocks, each approx. $1.5\,cm$-thick in sagittal direction. Blocks were frozen to $-80\,^{\circ}\mathrm{C}$, and up to five sections were cut from the face of each block using cryomicrotome. The $50\,\mu m$-thick slices were washed in 30% sucrose in sodium phosphate buffer (PBS), glass-mounted, stained for myelin with Sudan Black B, and scanned on a flat-bed scanner at 2000 dpi resolution ($12.7\,\mu m/pix$).

Registration: When serial sections and intermediate block-face images are not available, individual histological slices need to be registered directly to 3D MR volume. We designed an algorithmic framework for intensity-based slice-to-volume nonrigid registration with geometric transformation that combines an affine alignment with a 3D deformation field parameterized by thin-plate splines (TPS) [4]. Let $I((x,y) \in \Omega) \in \mathbb{R}$ and $V((x,y,z) \in \Phi) \in \mathbb{R}$ denote a 2D histological and a 3D MR image, respectively (the fourth degree B-spline interpolation model is used to obtain a continuous version from a discretized image). A geometric transformation $\mathscr{T}$ is defined as a mapping $\mathscr{T} : \Omega \mapsto \Phi$, which is composed of an affine transformation and a non-rigid deformation part: $\mathscr{T} = \mathscr{T}_{aff} \circ \mathscr{T}_{def}$. The non-rigid deformation is modeled by three independent TPS components defined on a common set of N control points (a regular grid). Thus, a geometric transformation $\mathscr{T}$ is parameterized by nine affine parameters (translation, rotation, scaling) and by 3D displacements of N control points, resulting in the total of $9+3N$ degrees of freedom. Let $Sim(I_1, I_2)$ denote an intensity-based similarity measure (a scalar) between two images I_1, I_2, such that closer similarity of images results in higher value. An example of a similarity measure is Pearson's correlation coefficient (CC) defined as:

$$S_{CC}(I_1, I_2) = \frac{\sum_i (I_1(i) - \langle I_1 \rangle)(I_2(i) - \langle I_2 \rangle)}{\sqrt{\sum_i (I_1(i) - \langle I_1 \rangle)^2 \sum_i (I_2(i) - \langle I_2 \rangle)^2}}, \qquad (1)$$

where brackets $\langle\rangle$ denote averaging. A cost function is defined as:

$$Cost(I, V, \mathscr{T}) = -Sim(I, V(\mathscr{T}(\Omega))) + \beta E(\mathscr{T}(\Omega)), \qquad (2)$$

where $E(\mathscr{T}(\Omega))$ is the transformation field energy penalty term with an associated weight parameter β, and $V(\mathscr{T}(\Omega))$ stands for the registered image (MRI slice). Image registration seeks the optimal transformation $\mathscr{T} = argmin(Cost(I, V, \mathscr{T}))$ that minimizes the cost function. An optimization algorithm finds an optimum in the multi-dimensional optimization landscape; we use the New Unconstrained Optimization Algorithm (NEWUOA) [5].

For registration, the MR image was preprocessed to correct for intensity inhomogeneities, and converted to an isotropic resolution of $0.35\,mm$. Histological images were converted to an 8-bit grey-scale intensity range (0 to 255), and re-sampled to match the spatial resolution of the MRI data; the bright background was suppressed by setting intensities above 240 to zero. Sections from eight coronal blocks of the brain were registered to MRI.

Selection of cortical ROIs: Several histological slices containing particular cortical ROIs were selected for further analysis. The ROIs were attributed anatomically by an expert neuroanatomist (FK), who traced prominent sulcal landmarks in the 3D MR image. Thus seven histological sections were selected that contained: 1) calcarine sulcus with striate cortex (three sections); 2) central sulcus with a fragment of the precentral bank (primary motor cortex) and postcentral bank (primary somatosensory cortex); 3) Heschl's gyrus (primary auditory cortex); 4) superior frontal gyrus; 5) middle frontal gyrus (see Fig. 1). For these sections, the best registration results were taken. In order to avoid possible blurring related to multiple interpolation/preprocessing steps, the registered images were computed directly from the original MR image using the fourth-order B-spline interpolation, a geometric transformation recovered by the registration being combined with all (reversed) pre-processing transformation steps. In the process, the registered MR images were supersampled to the pixel size of the histological images.

Intensity profiles: On image fragments with selected ROIs, two lines were manually drawn approximately delineating the pial and the grey/white matter (GM/WM) interface of the cortical ribbon. Wherever registration overlap of the cortex was very good (e.g., in the calcarine sulcus), lines were drawn only on a histological image and duplicated on a registered MR image. Curvilinear transcortical profiles were extracted using the Laplacian approach similar to a method first presented by Jones et al. [6]. In this method,

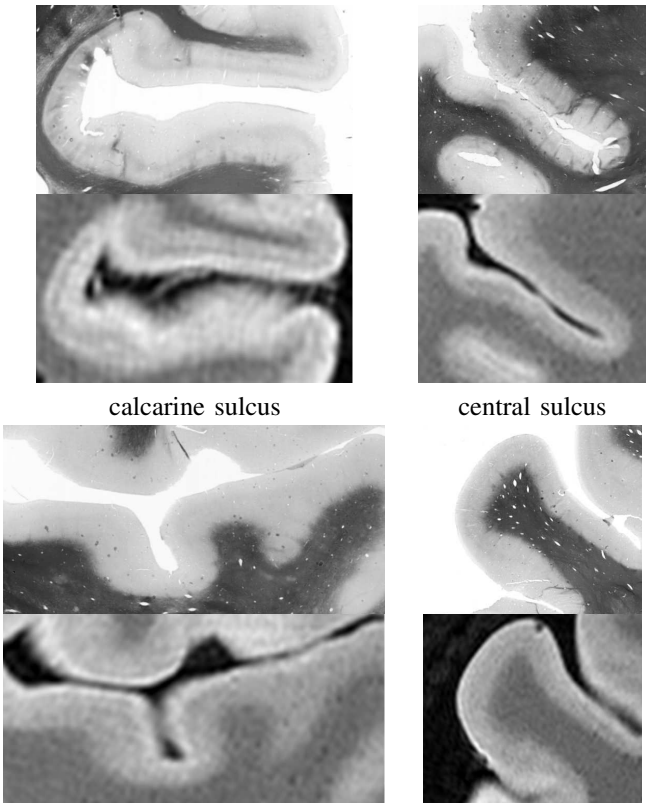

Fig. 1. Pairs of registered histological/MRI (top/bottom) slice fragments with selected regions of the cortex.

profiles are represented by curved trajectories of a Laplacian vector field, following the potential flow from one cortical surface to another. Such trajectories are orthogonal to all equipotential lines, which correspond to laminar layers, and are therefore optimal for capturing laminar patterns inside a convoluted ribbon. Laplace's partial differential equation (PDE) was solved in 2D on a uniform grid domain covering the cortical ROI, with a grid spacing matching the histological resolution. Boundary conditions were specified in the form of fixed potentials $U1$ and $U2$ at the outer and inner interface ($U1 > U2$). The potential field U satisfying Laplace's equation $\Delta U = \frac{\partial^2 U}{\partial x^2} + \frac{\partial^2 U}{\partial y^2} = 0$ was obtained as a steady state solution ($\frac{\partial U}{\partial t} \to 0$) of the heat equation $\frac{\partial U}{\partial t} = \Delta U$, which was solved numerically using a standard successive over-relaxation scheme with a forward-time-centered-space discretization. Profile lines were constructed by integration along the field gradient ∇U from the pial towards the GM/WM interface, using the second-order Runge-Kutta method; profiles were extracted with an inter-profile spacing of $\approx 80\,\mu m$ along the pial surface (see Fig. 2). Intensity values were sampled along a profile using spline interpolation. The intensity profiles, which have different lengths due to variable thickness of the cortex, were length-normalized by re-sampling to 300 points. In order to eliminate steep edges at transitions to background or WM, profiles were trimmed at both ends down to 256 points per profile. In addition,

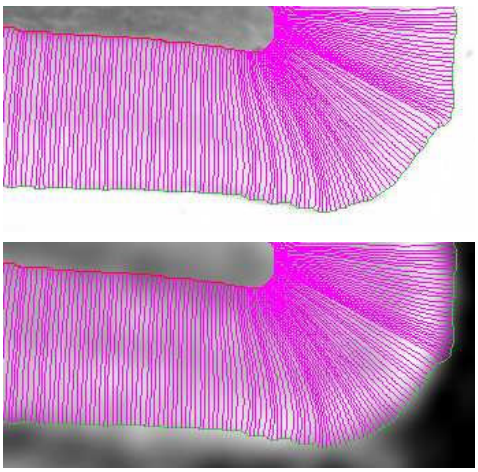

Fig. 2. Curvilinear transcortical profiles extracted by the Laplacian method, starting form pial interface towards grey/white matter interface (calcarine cortex; top: histology; bottom: MRI).

the histological profiles were corrected for an intensity slope due to bright background by subtracting a least-squares fitted line. The intensity values in each profile were z-normalized to zero mean and unit variance. Examples of intensity profile arrays are shown in the form of images in Fig. 3 (see section III).

Profile matching: Inter-modal comparison of profiles was performed in two stages: 1) templates were built by averaging of several adjacent histological profiles (as explained below); 2) templates were matched to MRI profiles by means of cross-correlational analysis. Since the histological images are usually corrupted by cuts, holes, staining artifacts, etc., and because of natural spatial variability of myelination patterns, each template source was constrained to a sufficiently large block (> 20 profiles) of adjacent profiles that were sufficiently similar to each other, as measured by Euclidean distance between normalized profile vectors. Thus, each template represented an average of a relatively uniform and uncorrupted block of histological profiles. A cross-correlation function was computed between a template and each MRI profile within a block spatially corresponding to the template source block, with an added overlap of 20 profiles on each side. Individual cross-correlation functions were combined using a non-linear combination scheme (further referred to as ML-XCORR) based on a maximum-likelihood approach [7]. ML-XCORR assumes the same statistical model that is typically used in a derivation of the cross-correlation optimality. An observed signal f (in our case, an MRI profile) is assumed to be a scaled (a_0) and shifted (s_0) version of a template signal g with an additive white Gaussian noise, i.e.

$$f(i) = a_0 g(i - s_0) + d_i, \quad d_i \sim N(0, \sigma_0^2), \quad i = 1..n. \qquad (3)$$

For simplicity, the signal f and template g are assumed to have a zero mean (in our case, this is guaranteed by the z-normalization). Under the assumed model, the likelihood defined as a function of model parameters (a, s, σ) is equal

to

$$L = \left(\frac{1}{\sqrt{2\pi\sigma^2}}\right)^n exp\left\{-\sum_{i=1}^{n}\frac{[f(i)-ag(i-s)]^2}{2\sigma^2}\right\}. \quad (4)$$

Out of all model parameters, we are interested in an estimate $\hat{s}$ of the true shift s_0 between signal and template. In our case, the shift parameter corresponds to a spatial lag between profiles of different modalities, which is possible due to errors in registration and/or manual tracing of interface lines. The intensity scaling parameter a is of less importance, because signal and template originate from different imaging modalities and are normalized by pre-processing. A maximum-likelihood (ML) estimate $\hat{s}$ of s is given by the maximum of the cross-correlation function $C(s)$ of f and g (see [7] for details), which is defined as

$$C(s) = \frac{1}{n\sqrt{var_f var_g}}\sum_i f(i)g(i-s), \quad (5)$$

where var_f and var_g denote variances of signal and template, respectively.

Suppose now that there are M signals f_k, $k = 1..M$; all are different realizations of the same stochastic model with the same template g and the same shift parameter s_0 (parameters a_k, σ_k may be different in each case). Cross-correlation functions $C_k(s)$ can be computed for each signal, yielding (slightly) different ML-estimates $\hat{s}_k$. The question is how to combine the cross-correlation functions into a single function, a maximum of which would give an estimate of the shift based on all observations. The simplest way is to combine them into the straightforward, non-weighted average [7]:

$$SA(s) = \frac{1}{M}\sum_{k=1}^{M} C_k(s). \quad (6)$$

Another popular way is to combine them as a weighted sum (each correlation term weighted by itself) into the determination coefficient (DC) [7]:

$$DC^2(s) = \frac{1}{M}\sum_{k=1}^{M} C_k^2(s). \quad (7)$$

A non-linear combination scheme (ML-XCORR) can be derived by the ML approach. The overall likelihood of the signals is:

$$L = \prod_{k=1}^{M}\left(\frac{1}{\sqrt{2\pi\sigma_k^2}}\right)^n exp\left\{-\sum_{i=1}^{n}\frac{[f_k(i)-a_k g(i-s)]^2}{2\sigma_k^2}\right\}. \quad (8)$$

It can be shown [7] that the likelihood function is maximized by the maximum of an 'effective' correlation function:

$$MX^2(s) = 1 - \left\{\prod_{k=1}^{M}\left[1-C_k^2(s)\right]\right\}^{1/M}. \quad (9)$$

The advantage of the above non-linear combination scheme is that cross-correlations corresponding to stronger signal-to-noise ratio (SNR) have a stronger impact, while cross-correlations with weaker SNR can be discarded. As shown in [7], this can be illustrated by the extreme cases: if one correlation term is close to unity (high SNR), then $MX(s)$ will be also close unity in spite of the other terms; if all correlation terms are small (low SNR), then $MX(s)$ approaches the determination coefficient $DC(s)$.

III. EXPERIMENTAL RESULTS

Registration performance was evaluated across a range of optimization algorithms (NEWUOA, Powell's direction set, Genetic, Levenberg-Marquardt, etc.), several intensity-based cost functions (CC, normalized mutual information, local correlation, etc.), and various classes of spline functions (TPS, Gaussian elastic body splines, cubic B-splines). For our data, a nonrigid registration algorithm using NEWUOA, a CC based similarity measure, and TPS deformation provided the best results (fastest processing and highest similarity score). When compared by an index computed on an areal overlap of a grey matter band, results of the nonrigid registration were substantially better than rigid registration. Registered histological and MRI slices (zoomed in to cortical ROI) shown on Fig. 1 visually demonstrate a good match. This method is more objective compared to [2], [3], where slices and ROIs are selected manually.

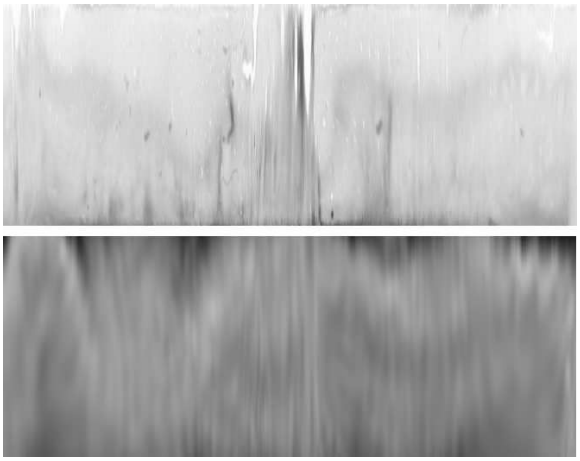

Fig. 3. Example of length-normalized intensity profiles shown in the form of images (calcarine cortex; top: histology; bottom: MRI).

Although we analyzed several cortical ROIs, further illustrations are limited to a single ROI and a single histological template profile due to limited space. The results of profile extraction are shown in the form of images in Fig. 3. In profiles extracted in the calcarine sulcus, there is a visually noticeable correspondence of a dark band (the stria of Gennari) in the second half (right part) of both histological and MRI profile arrays. An example of an average histological profile (template) is shown in Fig. 4; an average MRI profile constructed from a matching region is also shown for comparison. It can be seen that there are similar patterns in a histological and an MRI average profile with a noticeable shift between them.

Cross-correlation functions computed as described in section II and combined using all three above mentioned

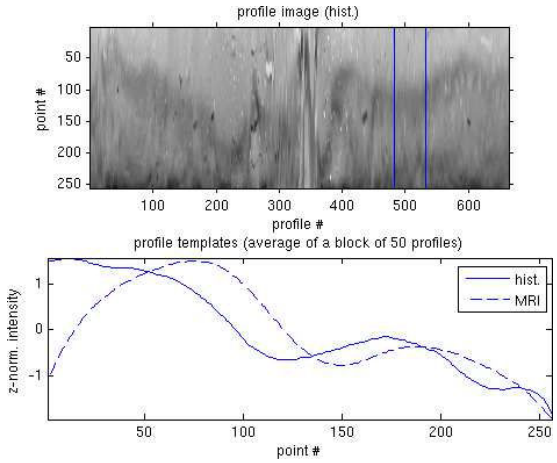

Fig. 4. Plot of average profile (*template*) (solid: histological, dash: MRI). Corresponding blocks of profiles used in template averaging are marked by vertical lines on the image (slope-corrected hist. profiles) above the plot.

schemes are shown in Fig.5. ML-XCORR method provides a higher and a more distinct peak (also true for other template regions not shown here); the location of a peak differs from that of in DC and SA scheme. Fig.5 also shows the central portions of templates matched by an ML-optimal shift determined by the ML-XCORR method. Pearson's correlation coefficient before/after shift was 0.798/0.992.

IV. CONCLUSION AND FUTURE WORKS

The results demonstrate that our method is capable of finding a close match in inter-modal intensity patterns across the cortex at locations whose spatial correspondence is established by image registration. Although the registration itself includes an intensity based similarity measure, a global smoothness constraint on the mapping does not guarantee the similarity of transcortical intensity profiles. The chosen method of cross-correlational analysis facilitates the detection of matching intensity profiles. The nonlinear scheme of combining per profile cross-correlation functions (ML-XCORR) ensures that individual profiles that bear higher correspondence to a template are weighted stronger in the cumulative measure. The results show that ML-XCORR scheme yields a more pronounced correlation peak compared to previous approaches. The shift parameter s accounts for a possible misalignment of profiles due to variations in tracing of interface lines and/or misregistration of cortical bands. The model of signal/template relationship can be augmented by another parameter, the length-scale b:

$$f(i) = ag(bi - s) + d_i, \quad d_i \sim N(0, \sigma^2), \quad i = 1..n. \qquad (10)$$

The length-scale parameter b accounts for a possible expansion/shrinkage of the pattern due to a difference in angles at which histological section and registered slice cut through the cortical layer. The augmented model can not be straightforwardly treated in the context of the ML-XCORR approach; it can be solved by a nonlinear optimization method. We are planning to evaluate the possible benefits of a template based nonlinear fitting routine.

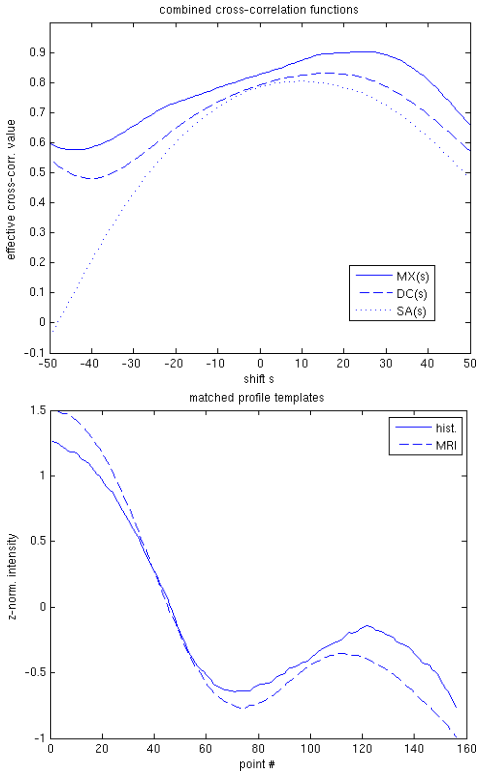

Fig. 5. Plots of effective cross-correlation functions (top) computed using three different schemes (MX,DC,SA) and central portions of profile templates (bottom) matched by the ML-optimal shift (25 pts.).

The available sample size is not sufficient for validation of close inter-modal correlates, but the image and signal processing context is reasonably well developed to allow the analysis of a larger sample group. Our method paves the way for further studies on quantitative comparison of high-resolution MRI and brain histology.

REFERENCES

[1] G.M. Fatterpekar, T.P. Naidich, B.N. Delman, J.G. Aguinaldo, S.H. Gultekin, C.C. Sherwood, P.R. Hof, B.P. Drayer, and Z.A. Fayad, "Cytoarchitecture of the human cerebral cortex: MR microscopy of excised specimens at 9.4 Tesla," *Am. J. Neuroradiol.*, vol. 23, pp. 1313-1321, 2002.

[2] J.C. Augustinack, A.J. van der Kouwe, M.L. Blackwell, D.S. Salat, C.J. Wiggins, M.P. Frosch, G.C. Wiggins, A. Potthast, L.L. Wald, and B.R. Fischl, "Detection of Entorhinal Layer II using 7 Tesla Magnetic Resonance Imaging," *Ann. Neurol.*, vol. 57, pp. 489-494, 2005.

[3] S. Eickhoff, N.B. Walters, A. Schleicher, J. Kril, G.F. Egan, K. Zilles, J.D. Watson, and K. Amunts, "High-resolution MRI reflects myeloarchitecture and cytoarchitecture of human cerebral cortex," *Human Brain Mapping*, vol. 24, pp. 206-215, 2005.

[4] F.L. Bookstein, "Principal warps: Thin-plate splines and the decomposition of deformations," *IEEE Trans. Patt. Anal. Machine Intell.*, vol. 11(6), pp. 567-585, 1989.

[5] M.J.D. Powell, "The NEWUOA software for unconstrained optimization without derivatives," *Cambridge, Numerical Anal. Group Tech. Report*, NA2004/08, pp. 1-42, 2004.

[6] S.E. Jones, B.R. Buchbinder, and I. Aharon, "Three-dimensional mapping of cortical thickness using Laplace's equation," *Human Brain Mapping*, vol. 11, pp. 12-32, 2000.

[7] S. Zucker, "Cross-correlation and maximum-likelihood analysis: a new approach to combining cross-correlation functions," *Mon. Not. R. Astron. Soc.*, vol. 342, pp. 1291-1298, 2003.